ELSEVIER

Journal of Alloys and Compounds 388 (2005) 250–257

Journal of ALLOYS AND COMPOUNDS

www.elsevier.com/locate/jallcom

Thermodynamic investigations of the Mn–Ni–C–N quarternary alloys by solid-state galvanic cell technique

Lidong Teng*, Ragnhild Aune, Seshadri Seetharaman

Department of Materials Science and Engineering, Royal Institute of Technology, Brinellvagen 23, SE-10044 Stockholm, Sweden

Received 19 June 2004; accepted 6 July 2004

Abstract

In view of the important applications of carbides and nitrides of transition metals in the hard materials industries, the thermodynamic activities of manganese in Mn–Ni–C–N alloys have been studied by solid-state galvanic cell technique with CaF_2 as the solid electrolyte. The phase compositions and microstructure of various alloys have been analyzed by X-ray diffraction (XRD) and scanning electron microscopy (SEM). Nitrogen was introduced into the alloy by equilibrating with N_2 gas. It was established during the experiments that the solubility of nitrogen in the alloys was affected by the carbon content. A $(Mn,Ni)_4(N,C)$ nitride was formed during the nitriding procedure in the alloys. The electromotive force (EMF) measurements were carried out in the temperature range 940–1127 K in order to determine the activities of Mn in the alloys. The activities of manganese were calculated and compared with those of the corresponding Mn–Ni–C ternary alloys.

Keywords: Interstitial alloys; Powder metallurgy; Scanning electron microscopy; Thermodynamics; Galvanic cell

1. Introduction

A study of the thermodynamic properties of transition metal systems containing nitrogen and carbon is a subject of considerable practical and theoretical interest. The thermodynamic properties of the Mn–Ni–C–N quaternary system are very important for the understanding of the properties of steels and hard materials. Even though the experimental information on phase diagrams for the Mn–Ni [1], Mn–C [2], Ni–C [3], Mn–N [4], Ni–N [5] binary systems was well-established, for some of the binary system, the calculated phase diagram still differs significantly with the experimental information. For instance, Huang [6] assessed the Mn–C systems. The calculated L/δ/γ equilibrium in this work was a eutectic instead of a peritectic one reported earlier. The calculated three-phase equilibrium of $Mn_{23}C_6/Mn_5C_2/Mn_7C_3$ at 701 K has not been reported experimentally. To the knowledge of the present authors, reliable and consistent experimental information is lacking for the corresponding ternary or quaternary systems. The thermodynamic properties of Mn–Ni–C system have been studied by the present authors [7]. In this paper, the alloys of the Mn–Ni–C–N quaternary system have been prepared by nitridation of the ternary alloys. The activities of manganese in these alloys have been studied by solid-state galvanic cell technique with CaF_2 single crystal as the electrolyte. This method has been reported to be a reliable method for the thermodynamic study of carbide systems [8–10].

2. Experimental

2.1. The alloy compositions and raw materials

The starting Mn–Ni–C alloy compositions and corresponding sample numbers (MNCN is the abbreviation of Mn–Ni–C–N system) are listed in Table 1. Fig. 1 illustrates the alloy compositions in the isothermal phase diagram of Mn–Ni–C system at 1123 K calculated by Thermo-Calc software [11]. Six alloys have been selected for the present study. The raw materials used in the preparation of the alloys, as well as for the electrodes, are listed in Table 2. The single

* Corresponding author.
E-mail address: lidongt@mse.kth.se (L. Teng).

0925-8388/$ – see front matter © 2004 Elsevier B.V. All rights reserved.
doi:10.1016/j.jallcom.2004.07.032

Table 1
The sample numbers, starting compositions (in mass%) of the Mn–Ni–C alloys and the main phases of the nitrided alloys determined by X-ray diffraction (XRD)

Sample no.	Ni	Mn	C	Main phases (XRD)
MNCN-11	10	86.8	3.2	γ, Mn_4N, $M_{23}C_6$
MNCN-13	30	67.6	2.4	γ, $M_{23}C_6$, M_4N
MNCN-21	10	84.4	5.6	γ, $M_{23}C_6$, M_4N
MNCN-22	20	75.1	4.9	γ, M_7C_3, M_4N
MNCN-33	30	64.2	5.8	γ, M_7C_3, graphite, M_4N
MNCN-42	20	69.7	10.3	γ, M_7C_3, graphite, M_4N

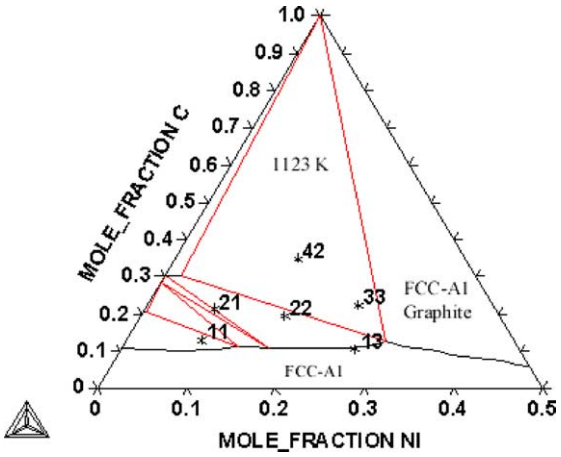

Fig. 1. The alloy compositions listed in Table 1 were located in the Mn–Ni–C isothermal phase diagram at 1123 K (calculated by Thermo-Calc [11]).

crystals of calcium fluoride (optical disk, 22 mm in diameter and 4 mm in thickness, polished both sides) were used as electrolytes that were supplied by Alfa Aesar. The argon and nitrogen gases used in the present work (99.9999%) were supplied by AGA Special Gas, Stockholm.

2.2. The cell arrangement

The galvanic cell used to determine the electromotive force (EMF) can be represented by the following schemes:

$$(-)\mathrm{Pt}, \mathrm{Mn} + \mathrm{MnF_2} + \mathrm{CaF_2}//\mathrm{CaF_2}//\mathrm{CaF_2} + \mathrm{MnF_2} + \underline{\mathrm{Mn}}\text{-alloy}, \mathrm{Pt}(+) \quad (1)$$

All the electrode components were in solid state. The individual electrode reactions can be written as follows:

$$\mathrm{Mn} + 2\mathrm{F}^- = \mathrm{MnF_2} + 2\mathrm{e}^- \quad \text{(left)} \quad (2)$$

Table 2
The raw materials used in the experiments

Name	Purity (mass%)	Particle size	Supplier
Mn powder	99.9	<150 μm	Alfa Aesar
Ni powder	99.8	<10 μm	Kebo Lab
Graphite powder	99.999	−325 mesh	Sigma–Aldrich
MnF_2 powder	98.0	Fine	Sigma–Aldrich
CaF_2 powder	99.95	−325 mesh	Alfa Aesar
Nitrogen gas	99.9999	–	AGA, Stockholm

$$\mathrm{MnF_2} + 2\mathrm{e}^- = \underline{\mathrm{Mn}}\text{-alloy} + 2\mathrm{F}^- \quad \text{(right)} \quad (3)$$

$$\mathrm{Mn} = \underline{\mathrm{Mn}}\text{-alloy} \quad \text{(overall)} \quad (4)$$

The molar Gibbs free energy change of reaction (4) is given by the Nernst equation [12]:

$$\Delta_4 G = -nEF = RT \ln a_{\underline{\mathrm{Mn}}\text{-alloy}} \quad (5)$$

where n denotes the number of electrons participating in the separate electrode reactions ($n = 2$ in Eq. (5)), F is the Faraday's constant, E is the electromotive force of the cell, R is the gas constant and T the temperature. It is important to point out that for Eq. (5) to be valid, the electrolyte must be a total ionic conductor and there must not be any side reaction occurring in the cell [9].

The galvanic cell assembly used for the electromotive force measurements was similar to that described in a previous work [7]. The single crystal CaF_2 electrolyte was kept sandwiched between the reference and working electrodes in an open cell arrangement. The cell was placed in a vertically mounted alumina reaction tube of a resistance furnace. The samples were positioned in the uniform temperature zone of the furnace (±0.5 K over a length of 6 cm). Due to the high oxygen affinity of Mn in the alloy [7], an oxygen partial pressure of less than 10^{-17} Pa was required to prevent the oxidation of Mn during the alloy synthesis as well as during the EMF measurement. Furthermore, as most of the carbides as well as CaF_2 are hygroscopic, the presence of moisture would affect the EMF measurements. As a result, the pure argon and nitrogen gases (99.9999%) were purified further by use of the gas cleaning system illustrated in Fig. 2. The argon gas was passed through columns of silica gel, ascarite and magnesium perchlorate to remove traces of H_2O and CO_2. The residual O_2 in the gas was removed by first passing the gas through a column of copper turnings at 873 K and later, through two columns of magnesium chips at 773 K (298 K for nitrogen gas). The oxygen partial pressure in the gas stream was monitored at all times, by passing the outgo-

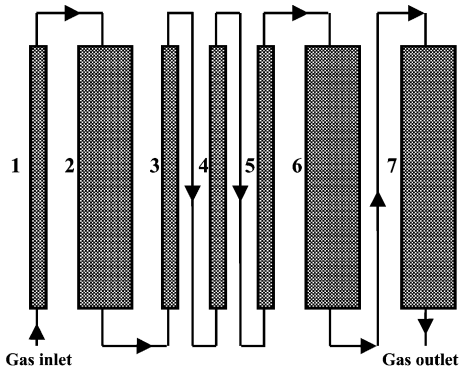

1. Silica gel
2. Copper turnings (873K)
3. Silica gel
4. Ascarite
5. Magnesium perchlorate
6, 7. Magnesium chips

Fig. 2. The schematic diagram of the argon and nitrogen gas cleaning system.

ing gas from the cell furnace containing the cell through an oxygen meter. The oxygen meter employed was built in the present laboratory using a ZrO_2–7.5 mol% CaO electrolyte tube with a slow stream of dry air as the reference electrode [13]. By carefully renewing the copper turnings and magnesium chips in the columns, the oxygen partial pressure in the gas stream was maintained to be less than 10^{-17} Pa. In addition to the purification of the argon before admission to the EMF apparatus, it was necessary to have internal getter for oxygen inside the enclosure housing of the cell. A titanium sponge placed in the path of the argon gas near the electrode served as the internal oxygen getter.

The molybdenum shield mounted inside the reaction tube was connected to ground potential in order to protect the cell from stray electrical disturbance. This shield served as an additional oxygen getter as well. The temperature of the cell was measured by a K-type thermocouple positioned under the cell. The thermocouple was calibrated against the melting point of pure gold. The reaction tube was closed at both ends with water-cooled copper lids provided with O-ring seals. The cell leads, the gas inlet and outlet tubes, as well as the thermocouple sheath, were taken out of the reaction tube through O-ring seals. The cell EMF was measured, to an accuracy of ±0.01 mV, by a digital Newport millivoltmeter. The reversibility of the cell was confirmed by polarizing the cell periodically and confirming that the cell returned to the equilibrium state.

2.3. Preparation of alloys and electrodes

Fine powders of Mn, Ni and graphite were mixed in required proportions (the mass ratio is shown in Table 1) to get the desired compositions. The mixtures were pressed into pellets, placed in alumina boats and sintered at 1273 K for 2 weeks under a stream of purified nitrogen gas at 1 atm. The samples were cooled in the furnace. Some of the samples were crushed and ground well to prepare the electrodes. The samples for X-ray diffraction (XRD) and scanning electron microscopy (SEM) examination were heated at 1123 K in 1 atm N_2 gas and held for 336 h and then quenched in liquid nitrogen. The quenched samples were examined by XRD to confirm the existence of the expected phases and by SEM to analyze the equilibrium phase compositions. The samples were analyzed for carbon by the combustion method using a LECO carbon analyzer and the carbon contents obtained were within ±3% of the weighed in amounts.

The alloy powders were mixed with MnF_2 and CaF_2 in the weight ratio of 75:15:10. The mixtures were compacted into cylindrical pellets with a diameter of 16 mm and a thickness of 3 mm (3–4 g). In view of the hygroscopic nature of the electrode components, all the above operations were carried out in a dry argon glove-box. The pellets were sintered in boron nitride crucibles at 1173 K for 4 h in an atmosphere of purified argon before being mounted in the galvanic cell. The reference electrodes, consisting of fine powders of pure Mn, MnF_2 and CaF_2, were also mixed in the mass ratio of 75:15:10 and prepared as indicated above. Visual examination of the sintered electrodes did not show any sign of oxidation. An analysis of the carbon content of the alloy electrode after sintering showed that there was no carbon loss during the preparation of the electrode.

2.4. EMF measurement procedure

After the cell was mounted inside the reaction tube, the system was evacuated at 423 K for 12 h at a pressure of 1.0 Pa to remove the moisture absorbed in the ceramic components around the cell. This vacuum-drying process was found to be of great importance in improving the accuracy of the EMF measurement. When the oxygen sensor, that monitored the partial pressure of oxygen in the outgoing gas, showed a value less than 10^{-17} Pa, the furnace was started. The cell temperature was raised to 1073 K over a period of 4 h. While the time needed for the cell to obtain equilibrium was about 48 h in the first heating, the equilibrium time thereafter changed with temperature. In general, the EMF values were considered to be stable if they were constant within ±0.2 mV over a period of 3 h. The measurements were made at temperature intervals of about 30 K, and the cell was taken through several temperature cycles. Each measurement lasted about 8 days. The cell measurements were repeated in a number of cases in order to check the reproducibility of the EMF values obtained previously.

3. Results and discussions

3.1. Phase composition and microstructure

The phase compositions of all the alloys annealed at 1123 K were analyzed by use of the XRD method. In Fig. 3(a–c), the XRD patterns of the MNCN-11, MNCN-33 and MNCN-42 alloys are shown. It can be seen from the figures that the main phases in the MNCN-11 are γ-(MnNi), $(Mn,Ni)_4N$ and $(MnNi)_{23}C_6$. The main phases in the MNCN-33 and MNCN-42 alloys are γ-(Mn,Ni), $(Mn,Ni)_7C_3$, graphite and $(Mn,Ni)_4N$. The main phases of all the other studied alloys, identified by XRD at room temperature, are listed in Table 1. The microstructure of the MNCN-11 alloy annealed in 1 atm N_2 at 1123 K/336 h is shown in Fig. 4(a and b). In Fig. 4(a), the light grey matrix phase are γ and M_4N (M denotes the mixture of Mn and Ni), the round deep-grey phase are $M_{23}C_6$, and the black droplets are cavities. As shown in Fig. 4(b), the nitride phase M_4N was formed in the solid solution of Mn and Ni. The microstructure of the MNCN-33 alloy is shown in Fig. 5(a and b). In Fig. 5(a), light grey matrix phases are γ and M_4N, the black phase is M_7C_3, the dark areas are cavities. It can be seen from Fig. 5(b) that the nitrogen could dissolve into the solid solution phase and form nitride particles with the formula M_4N. The phase compositions were analyzed by electron microprobe JEOL 8900R and JESM 840. Experimentally determined phase composi-

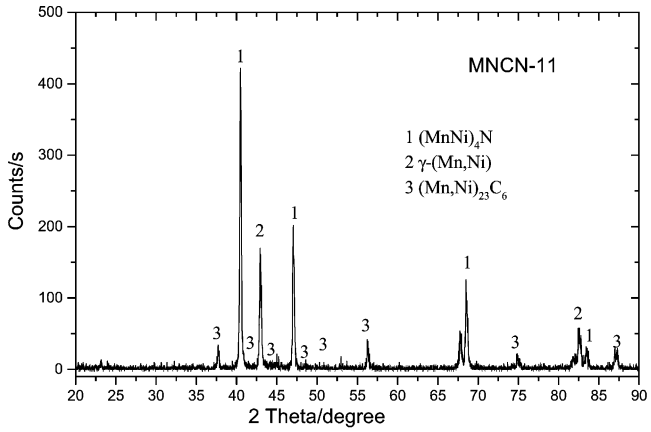

(a)

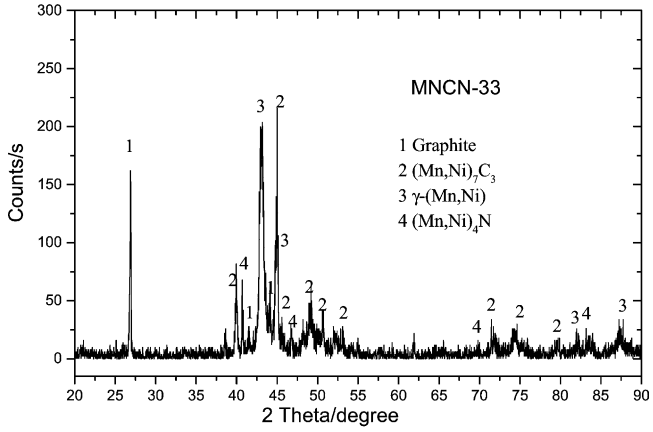

(b)

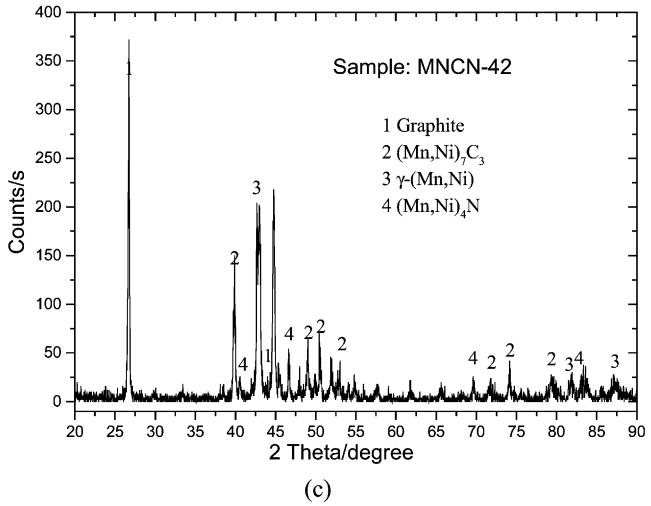

(c)

Fig. 3. The XRD patterns of the MNCN-11, MNCN-33 and MNCN-42 alloys quenched at 1123 K. (a) MNCN-11 alloy, (b) MNCN-33 alloy, (c) MNCN-42 alloy.

tions in the Mn–Ni–C–N system annealed in 1 atm N_2 at 1123 K/336 h are shown in Table 3. Chemical composition is given in site fractions of metal components y_{Mn} and y_{Ni} ($y_i = x_i/(x_{Mn} + x_{Ni})$; x_i molar fraction of element). As can be

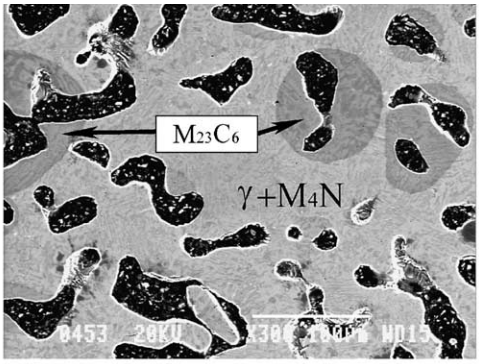

(a)

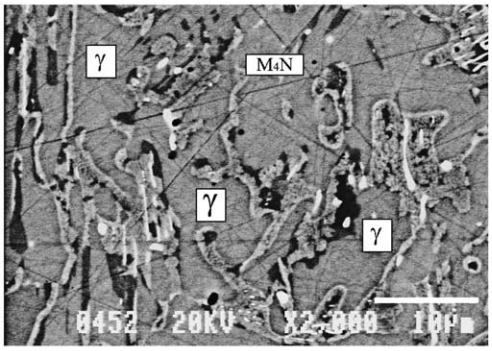

(b)

Fig. 4. Microstructure of MNCN-11 annealed in 1 atm N_2 at 1123 K/336 h. (a) The light-grey matrix phases are γ and M_4N, the round deep-grey phase is $M_{23}C_6$, the black droplets are cavities; (b) the magnification photo of the light-grey matrix phase in (a).

Table 3
Experimentally determined phase compositions in the Mn–Ni–C–N equilibrium system annealed in 1 atm N_2 at 1123 K/336 h

Specimens	Phases	y_{Mn}	y_{Ni}
MNCN-11	γ	0.872	0.128
	$M_{23}C_6$	0.988	0.011
	M_4N	0.918	0.082
MNCN-13	γ	0.633	0.367
	$M_{23}C_6$	0.989	0.011
	M_4N	0.915	0.085
MNCN-21	γ	0.653	0.347
	$M_{23}C_6$	0.989	0.011
	M_4N	0.917	0.083
MNCN-22	γ	0.596	0.404
	M_7C_3	0.982	0.018
	M_4N	0.929	0.071
MNCN-33	γ	0.514	0.486
	M_7C_3	0.975	0.025
	M_4N	0.934	0.066
	Graphite	0.000	0.000
MNCN-42	γ	0.518	0.482
	M_7C_3	0.977	0.023
	M_4N	0.945	0.055
	Graphite	0.000	0.000

Chemical composition is given in site fractions of metal components y_{Mn} and y_{Ni} ($y_i = x_i/(x_{Mn} + x_{Ni})$; x_i molar fraction of element).

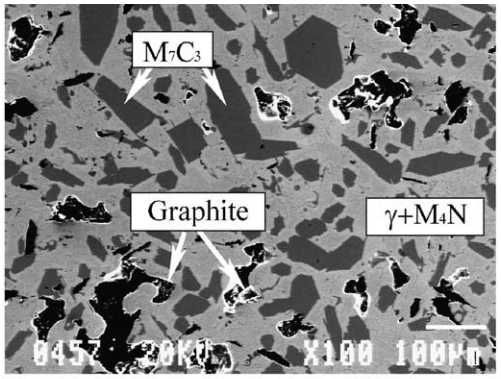

(a)

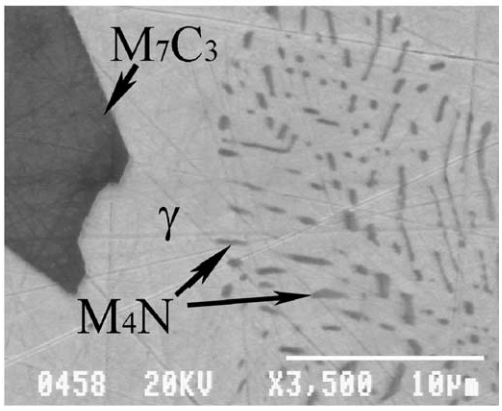

(b)

Fig. 5. Microstructure of MNCN-33 alloy annealed in 1 atm N_2 at 1123 K/336 h. (a) The light grey matrix phases are γ and M_4N, the black phase is M_7C_3, the dark phase is cavities; (b) the magnification photo of the light-grey matrix phase in (a), the deep-grey droplets are M_4N.

seen from Table 3, the site fractions of Mn and Ni in $M_{23}C_6$ or M_7C_3 are nearly constant in the different alloys. Further, the solubility of Ni in the carbides is quite low and the value is less than 2%. The solubility of Ni in the M_4N phase is about 6–8%. Mn and Ni can form continuous series of solid solutions in the quarternary alloys. The nitrogen content in the nitride for alloys MNCN-13 and MNCN-21 is shown in Table 4. The molar fraction of N in the M_4N is about 0.09 for both of the alloys. The compositions of nitrides in the two different alloys were quite similar and they are close to the stoichiometrical composition of Mn_4N. It can be seen from the XRD and SEM analyses results that alloys MNCN-33 and MNCN-42 are in the same four-phase region and the phase compositions are independent of the alloy composition in this region of the Mn–Ni–C–N quarternary system.

Table 4
The phase compositions of MNCN-13 and MNCN-21 alloys annealed in 1 atm N_2 at 1123 K/336 h

Specimens	Phases	x_{Mn}	x_{Ni}	x_C	x_N
MNCN-13	γ	0.62	0.36	0.02	–
	$M_{23}C_6$	0.86	0.01	0.13	–
	M_4N	0.76	0.07	0.08	0.09
MNCN-21	γ	0.64	0.34	0.02	
	M_7C_3	0.88	0.01	0.11	
	M_4N	0.78	0.07	0.06	0.09
	Graphite			1.00	

Analyzed by electron microprobe JEOL 8900R, in mole fraction x_i.

3.2. Thermodynamic activities of Mn in Mn–Ni–C–N alloys

It is assumed that the standard state for Mn is pure β-Mn in the calculation of manganese activity. The experimentally determined EMF values in the temperature range from 940 K to 1127 K for the different alloys are presented in Table 5. It is to be noted that the EMF values in Table 5 are the average values of a number of measurements during several heating and cooling cycles for all the experiments with the particular alloy. The standard deviation was found to be less than ±1.6 mV. The activities of Mn in the Mn–Ni–C–N alloys have been calculated by using Eq. (5) and the calculated results are shown in Fig. 6. The three points corresponding to alloy MNCN-11 at 1094 K and 1095 K are values repeated after a temperature-cycling from 1094 K down to 952 K and then back up to 1095 K. It can be seen that the experimental values measured at 1094 K and 1095 K are in good agreement with each other confirming that the experimental results were reproducible and the galvanic cell was in equilibrium. The activities of Mn increase with increasing temperature for the MNCN-11 alloy in the range of 952–1126 K. The similar relationship between the activity of Mn and temperature for the other alloys can be seen from Fig. 6. The activities of Mn for alloy MNCN-33 fall very close to those for alloy MNCN-42, as can be seen in Fig. 6. The largest difference between these two sets of values at the same temperature is less than 3%. It is reasonable to assume that these two alloys are in the same four-phase region and the activities of components are independent of the alloy composition in this region of the Mn–Ni–C–N quarternary system. This result is in conformity with the phase composition analysis in Section 3.1.

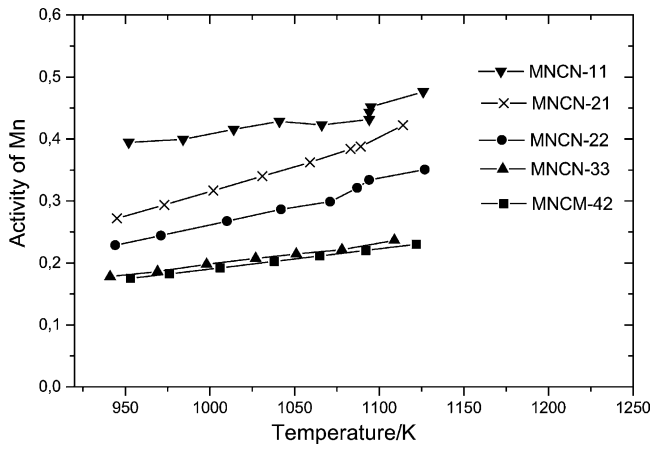

Fig. 6. Plots of activity of Mn against the equilibrium temperature of the selected alloys.

Table 5
The experimental results of EMF (mV) measured at the temperature range from 941 K to 1127 K for the Mn–Ni–C–N alloys

MNCN-11		MNCN-21		MNCN-22		MNCN-33		MNCN-42	
T (K)	EMF	*T* (K)	EMF	*T* (K)	EMF	*T* (K)	EMF	*T* (K)	EMF
952	38.13	945	53.00	944	60.01	941	69.95	953	71.49
984	38.89	973	51.37	971	58.98	969	70.16	976	71.56
1014	38.35	1002	49.63	1010	57.39	998	69.66	1006	71.52
1041	38.01	1031	47.92	1042	56.13	1027	69.61	1038	71.42
1066	39.53	1059	46.32	1071	55.73	1051	69.72	1065	71.31
1094	39.61	1089	44.44	1087	53.20	1078	70.05	1092	71.19
1094	38.36	1114	41.39	1094	51.69	1109	68.87	1122	70.99
1095	37.48			1127	50.86				
1126	35.99								

The agreement of Mn activities for the alloys MNCN-33 and MNCN-42 in two different measurements also demonstrates that the experimental results are quite reproducible.

To identify the phase transformation of the alloy during the EMF measurements, differential thermal analysis (DTA) was carried out in the temperature range 298–1373 K. Fig. 7 shows the DTA curves for the alloys MNCN-11 and MNCN-33. There is one endothermal peak at 1126 K for alloy MNCN-11 and it is related to the phase transformation of solid solution β → γ. In alloy MNCN-33, there are two peaks in the DTA curves. The endothermal peak at 933 K is likely to be caused by the transformation α → β and the peak at 1235 K is due to β → γ. The DTA curves for other alloys have not been included in this paper, but the corresponding endothermic-peak temperatures are shown in Table 6. Further experimentation by alloy-quenching method is needed to get detailed phase change information.

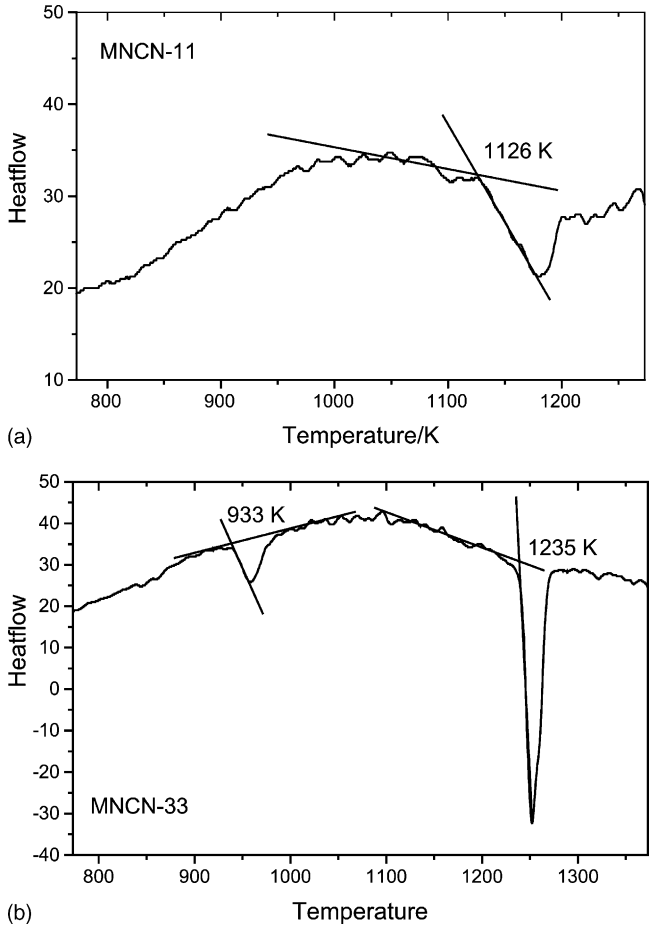

Fig. 7. DTA curves of alloys MNCN-11 and MNCN-33. (a) MNCN-11, (b) MNCN-33.

3.3. The effect of N on the activity of Mn

The activities of manganese for the alloys MNC-11 (MNC is the abbreviation of the matrix alloy of Mn–Ni–C system which has not been reacted with nitrogen) and MNCN-11 are shown in Fig. 8. In this figure, the Mn activities in MNC-11 are higher than the values in MNCN-11. The addition of N to the Mn–Ni–C ternary alloys decreases the activity of manganese. The negative effect of N on the activity of Mn in the quarternary system Mn–Ni–C–N does, however, decrease as the carbon content increases. When the alloy was saturated in the carbon and graphite existed as a stable phase in the alloy, the effect of N on the activity of Mn is not significant. Fig. 9 shows the activities of Mn measured in the matrix alloy MNC-42 and nitrided alloy MNCN-42. The activities of Mn in the unnitrided alloy MNC-42 are quite close to those in the nitrided alloy MNCN-42 with only maximum 2% difference. This result shows that the solubility of nitrogen in the carbon-saturated alloys is very low. The standard Gibbs free energy of formation per mole Mn, $\Delta G^{0}_{m,Mn}$, for Mn_7C_3,

Table 6
The endothermic peaks in the DTA curves for the alloys and the possible phase transformation

Sample no.	Phase transformation and temperature, *T* (K)		
	α → β	β → γ	γ → δ
MNCN-11		1126	
MNCN-13	929	1096	1247
MNCN-21		1101	1286
MNCN-22	925		1276
MNCN-33	933		1238
MNCN-42	981	1141	1276

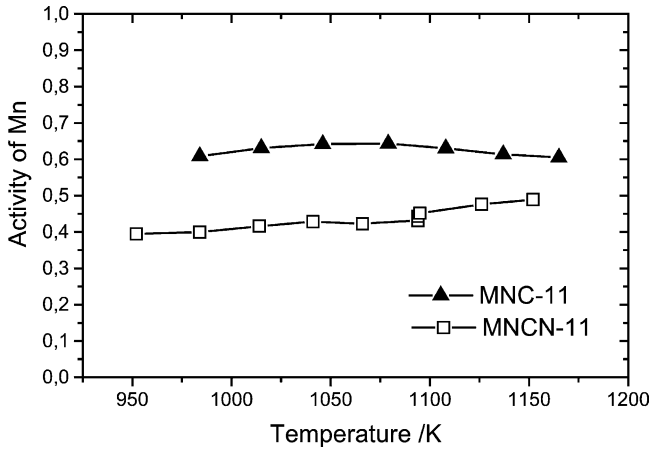

Fig. 8. Plot of manganese activity against temperature for the MNC-11 and MNCN-11 alloys.

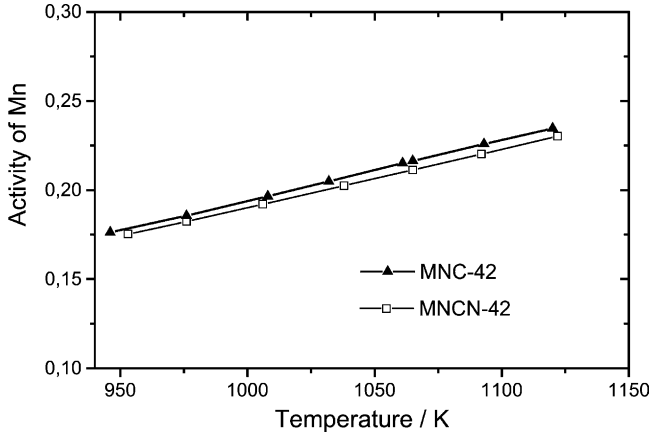

Fig. 9. Plot of manganese activity against temperature for the MNC-42 and MNCN-42 alloys.

Mn_5N_2 and Mn_4N in the temperature range of 300–1200 K is shown in Fig. 10. It can be seen from Fig. 10 that the Mn_7C_3 is more stable than the manganese nitrides when the temperature is over 800 K, while the manganese nitrides are more stable than manganese carbides below 800 K. Thus, the interaction between Mn and N is likely to be weaker than that between Mn and C at higher temperatures. As a result, when the carbon content in the alloys is low, $(Mn,Ni)_4(N,C)$ could form during the nitridation process. When the carbon is saturated and the graphite existed in the alloy, the manganese would preferentially combine with carbon and the formation of $(Mn,Ni)_4(N,C)$ phase would be hindered. This result is demonstrated by the XRD analysis, as discussed earlier. The main phase of alloy MNCN-11 was $(Mn,Ni)_4(N,C)$, while in alloy MNCN-42, only small amount of nitride phase of $(Mn,Ni)_4N$ could be detected by the XRD analysis.

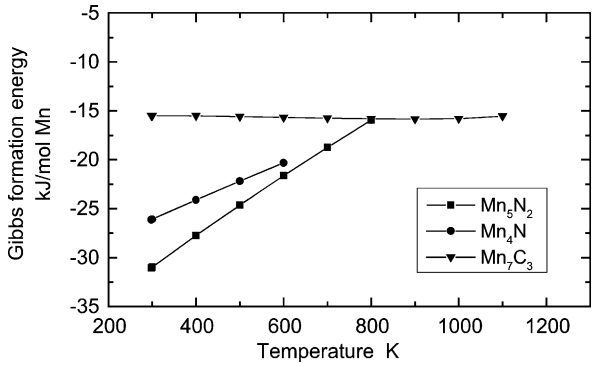

Fig. 10. The standard free energy of formation per molar Mn for Mn_7C_3, Mn_5N_2 and Mn_4N in the temperature range of 300–1200 K.

4. Conclusions

The Mn–Ni–C–N alloys have been prepared by N_2 gas nitridation process with the Mn–Ni–C alloys. Electromotive force measurements were carried out in the temperature range 940–1127 K by solid-state galvanic cell technique with CaF_2 as the solid electrolyte. It was established that the solubilities of nitrogen in the alloys were affected by the carbon contents. The XRD results show that a $(Mn,Ni)_4(N,C)$ nitride was formed during the nitriding procedure in the alloys. The site fraction of Ni in the nitride compounds is about 0.08. The site fraction of Ni in $M_{23}C_6$ is about 0.011 and that in M_7C_3 is about 0.025. The addition of N to the Mn–Ni–C ternary alloys was found to decrease the activity of manganese. However, in the case of carbon-saturated alloys, the effect of N on the activity of Mn is insignificant. The thermodynamic data obtained by this study will be used in the assessment of Mn–Ni–C–N quaternary system.

Acknowledgements

The authors wish to thank Professor Wenchao Li for his valuable help and suggestions during this work. Financial support for this work from the Swedish Research Council (VR) is gratefully acknowledged.

References

[1] T.B. Massalski, Binary Phase Diagrams, second ed., ASM International, Materials Park (OH), 1990, p. 2582.
[2] T.B. Massalski, Binary Phase Diagrams, second ed., ASM International, Materials Park (OH), 1990, p. 860.
[3] T.B. Massalski, Binary Phase Diagrams, second ed., ASM International, Materials Park (OH), 1990, p. 867.
[4] C. Qiu, A. Fernandez Guillermet, Z. Metallkd. 84 (1993) 11–16.
[5] K. Frisk, Int. J. Thermophys. 12 (1990) 417–422.
[6] W.M. Huang, Scand. J. Metall. 19 (1990) 26–30.
[7] L.D. Teng, R. Aune, S. Seetharaman, Intermetallics 11 (2003) 1229–1235.
[8] J.W. Hinze, J.W. Patterson, J. Electrochem. Soc. 120 (1973) 96–100.
[9] K. Kiukkola, C. Wagner, J. Electrochem. Soc. 104 (1957) 308–312.
[10] S. Du, S. Seetharaman, L.-I. Staffansson, Metall. Trans. B 20 (1989) 747–751.

[11] Thermocalc Software, version P on WinNT, 2000, http://www.thermocalc.com.
[12] E.C. Subbarao, Solid Electrolytes and their Applications, Plenum Press, New York, 1980, p. 257.
[13] S. Seetharaman, S.C. Du, A. Jakobsson, in: R.G. Reddy, J.C. Males (Eds.), Sensors and Modeling in Materials Processing: Techniques and Applications, The Mineral, Metals & Materials Society, 1997, p. 327.